Fast energy transfer mediated by multi-quanta bound states in a nonlinear quantum lattice

Cyril Falvo, Vincent J.C. Pouthier, J. C. Eilbeck

Fast energy transfer mediated by multi-quanta bound states in a nonlinear quantum lattice

C. Falvo and V. Pouthier

CNRS UMR6624, Université de Franche Comté, Laboratoire de Physique Moléculaire, 25030 Besançon cedex - France

J. C. Eilbeck

Department of Mathematics, Heriot-Watt University, Riccarton, Edinburgh, EH14 4AS - UK

Abstract

By using a Generalized Hubbard model for bosons, the energy transfer in a nonlinear quantum lattice is studied, with special emphasis on the interplay between local and nonlocal nonlinearity. For a strong local nonlinearity, it is shown that the creation of v quanta on one site excites a soliton band formed by bound states involving v quanta trapped on the same site. The energy is first localized on the excited site over a significant timescale and then slowly delocalizes along the lattice. As when increasing the nonlocal nonlinearity, a faster dynamics occurs and the energy propagates more rapidly along the lattice. Nevertheless, the larger is the number of quanta, the slower is the dynamics. However, it is shown that when the nonlocal nonlinearity reaches a critical value, the lattice suddenly supports a very fast energy propagation whose dynamics is almost independent on the number of quanta. The energy is transfered by specific bound states formed by the superimposition of states involving $v - p$ quanta trapped on one site and p quanta trapped on the nearest neighbour sites, with $p = 0, .., v - 1$. These bound states behave as independent quanta and they exhibit a dynamics which is insensitive to the nonlinearity and controlled by the single quantum hopping constant.

Key words: Nonlinear quantum lattice; Quantum breather; Bound state

1 Introduction

The concept of energy localization due to nonlinearity in classical lattices has been a central topic of intense research over the last three decades. This topic can be traced back to the seminal works of Davydov, where the nonlinearity

was introduced to explain the vibrational energy flow in α-helices [1]. The main idea was that the energy released by the hydrolysis of adenosine triphophate (ATP), partially stored in the high-frequency amide-I vibration of a peptide group, delocalizes along the helix leading to the formation of vibrational excitons. Due to their interaction with the phonons of the helix, the excitons experience a nonlinear dynamics. Therefore, they propagate according as a "Davydov" soliton, a solution of the Nonlinear Schrödinger (NLS) equation within the continuum approximation [2,3]. In the mid-1980's, lattice effects were introduced through the analysis of the discrete version of NLS. This equation supports specific solutions called "lattice solitons" [4] and it has revealed the occurrence of a remarkable feature known as the self-trapping mechanism [5]. As discovered by Sievers and Takeno [6], the self-trapping is a special example of a more general solutions called discrete breathers [7,8,9]. In classical anharmonic lattices, a discrete breathers correspond to time-periodic and spatially localized solutions which result from the interplay between the discreteness and the nonlinearity. These solutions do not require integrability for their existence and stability and it has been suggested that they should correspond to quite general and robust solutions. Since discrete breathers sustain a local accumulation of the vibrational energy, which might be pinned in the lattice or may travel through it, they are expected to be of fundamental importance.

At present, because the occurrence of classical breathers is a relatively well understood phenomena, great attention has been paid to characterize their quantum equivalent, for which less detailed results are known [10]. In the quantum regime, the Bloch theorem applies due to the translational invariance of the lattice. Therefore, the corresponding eigenstates cannot localize the energy because they must share the symmetry of the translation operator which commutes with the lattice Hamiltonian. Nevertheless, the nonlinearity is responsible for the occurrence of specific states called multi-quanta bound states [10,11,12,13,14,15,16,17,18,19,20,21,22,23,24,25,26,27]. A bound state corresponds to the trapping of several quanta over only a few neighbouring sites, with a resulting energy which is less than the energy of quanta lying far apart. The distance separating the quanta is small, so that they behave as a single particle delocalized along the lattice with a well-defined momentum. Since the occurrence of these bound states results from the nonlinearity, they can be viewed as the quantum counterpart of breathers or solitons. In low-dimensional lattices, two-quanta bound states have been observed in molecular adsorbates such as H/Si(111) [28,29], H/C(111) [30], CO/NaCl(100) [31] and CO/Ru(001) [32,33,34,35,36] using optical probes. Bound states in the system H/Ni(111) were investigated via high resolution electron energy loss spectroscopy [37]. Moreover, a recent experiment, based on femtosecond infrared pump-probe spectroscopy, has clearly established the existence of bound states in α-helices [38].

From a theoretical point of view, most of the previous work was performed within the quantum equivalent of the discrete NLS equation. The corresponding Hamiltonian is essentially a Bose version of the Hubbard model which has been used to study a great variety of situations ranging from molecular lattices [11] to Bose-Einstein condensates [39,40,41]. Within this model, the nonlinearity is local so that it is responsible for a strong interaction between quanta located on the same site. However, through the small polaron description of the vibrational energy flow in proteins, it has been shown recently that a nonlocal nonlinearity strongly modifies the nature of the bound states [22,23,24,25,42]. In such systems, the polaron results from the dressing of a vibrational exciton by a virtual cloud of phonons. In addition to an attractive coupling between polarons located onto the same site, a coupling takes place when polarons lie on nearest neighbour sites, due to the overlap between their virtual cloud of phonons. When two quanta are excited, the competition between the local and the nonlocal nonlinearity favours the occurrence of two kinds of bound states whose properties have been discussed in details in Ref. [22].

At this step, the fundamental question arises whether the interplay between the local and the nonlocal nonlinearity modifies the dynamics of bound states involving several quanta. This is the purpose of the present paper. It will be shown, using a generalized Hubbard model, that a critical value of the nonlocal nonlinearity favours a resonance responsible for a fast energy transfer. Note that, although such an approach is rather general, it will be applied to vibrational excitons moving in a nonlinear molecular lattice.

The paper is organized as follows. In Section 2, the generalized Hubbard model is described and the number state method [17], used to define its eigenstates, is summarized. Then, the quantum dynamics required to characterize the transport properties is introduced. The corresponding time dependent Schrödinger equation is solved numerically in Section 3 where a detailed analysis of the multi-quanta dynamics is performed. Finally, the numerical results are discussed and interpreted in Section 4.

2 Model Hamiltonian and Quantum analysis

2.1 Hamiltonian and Quantum states

We consider a one-dimensional lattice formed by N sites whose position is defined in terms of the integer index n. Each site n is occupied by a high-frequency oscillator described by the standard boson operators $b_n^\dagger$ and b_n. The lattice dynamics is governed by a generalized Hubbard model for bosons whose

Hamiltonian is written as (using the convention $\hbar = 1$)

$$H = \sum_n \omega_0 b_n^\dagger b_n - A b_n^\dagger b_n^\dagger b_n b_n - B b_{n+1}^\dagger b_n^\dagger b_{n+1} b_n + \Phi[b_n^\dagger b_{n+1} + b_{n+1}^\dagger b_n] \qquad (1)$$

where ω_0 is the internal frequency of each oscillator, Φ is the hopping constant between nearest neighbour sites, and A and B represent the local and the nonlocal nonlinearity, respectively. Note that for vibrational excitons, the nonlinear parameters are positive.

Since the Hamiltonian H (Eq.(1)) conserves the number of quanta, its eigenstates can be determined by using the number state method detailed in Ref. [17]. This method is summarized as follows. Because H commutes with the operator $\sum_n b_n^\dagger b_n$ which counts the total number of quanta, the Hilbert space E is written as the tensor product $E = E_0 \otimes E_1 \otimes E_2 \otimes ... \otimes E_v ...$, where E_v refers to the v-quanta subspace. To generate E_v, a useful basis set is formed by the local vectors $|p_1, ..., p_N\rangle$ ($\sum_n p_n = v$), where p_n is the number of quanta located on the nth site. The dimension d_v of E_v is equal to the number of ways of distributing v indistinguishable quanta among N sites, i.e. $d_v = (N + v - 1)!/v!(N - 1)!$.

Within this representation, the Hamiltonian is block-diagonal. However, the size of each block can be reduced by taking advantage of the lattice periodicity. Indeed, due to the translational invariance, the lattice momentum k is a good quantum number so that an "momentum" basis set can be formed. For each k value, an momentum vector $|\Phi_\alpha(k)\rangle$ is obtained by superimposing all the vectors $|p_1, ..., p_N\rangle$ describing similar quanta distributions related to each other by a translation along the lattice. For instance, the momentum vector built from the N vectors $|v, 0, ..., 0\rangle$, ... , $|0, 0, ..., v\rangle$ is defined as

$$|\Phi_1(k)\rangle = \frac{1}{\sqrt{N}} \sum_{n=0}^{N-1} e^{ikn} T^n |v, 0, ..., 0\rangle \qquad (2)$$

where the translation operator T satisfies $T|p_1, p_2 ..., p_N\rangle = |p_N, p_1 ..., p_{N-1}\rangle$.

Consequently, in each subspace E_v, the Hamiltonian exhibits independent blocks associated to each k value and the corresponding Schrödinger equation can be solved with a minimum of computational effort. This numerical procedure yields the eigenvalues $\omega_\lambda^{(v)}(k)$, which define the dispersion relations of the v-quanta subspace, and the associated eigenvectors $\Psi_\lambda^{(v)}(k)$.

2.2 Quantum dynamics

The quantum dynamics is governed by the time dependent Schrödinger equation written as

$$i\frac{d|\Psi(t)\rangle}{dt} = H|\Psi(t)\rangle \tag{3}$$

where $|\Psi(t)\rangle$ is the lattice quantum state at time t. By assuming that the state is known at the initial time $t = 0$, its value at time $t > 0$ is expressed in terms of the eigenstates of H as

$$|\Psi(t)\rangle = \sum_{v}\sum_{k\lambda}\langle\Psi_{\lambda}^{(v)}(k)|\Psi(0)\rangle e^{-i\omega_{\lambda}^{(v)}(k)t}|\Psi_{\lambda}^{(v)}(k)\rangle \tag{4}$$

The time dependent quantum state $|\Psi(t)\rangle$ is the central object of the present study. Its knowledge allows us to characterize the multi-quanta dynamics through the computation of the expectation value of any relevant observable O as $\langle O(t)\rangle = \langle\Psi(t)|O|\Psi(t)\rangle$. Nevertheless, the solution of Eq.(4) requires the specification of an initial quantum state. To proceed, we restrict our attention to a spatially localized state corresponding to the creation of v quanta on the n_0th site as

$$|\Psi(0)\rangle = \frac{b_{n_0}^{\dagger v}}{\sqrt{v!}}|0\rangle \tag{5}$$

where $|0\rangle$ denotes the vacuum with zero quanta. This specific choice allows us to characterize the ability of the nonlinear quantum lattice to localize the energy, at least over a given timescale. Indeed, for a vanishing nonlocal nonlinearity ($B = 0$), each subspace E_v supports a low energy band called the soliton band [16,17]. For vibrational excitons, the nonlinearity A is usually greater than the hopping constant Φ. Consequently, the soliton band describes v-quanta bound states in which the v quanta are trapped on the same site and behave as a single particle. When v quanta are created on a given state, only the soliton band is significantly excited. Because the dispersion of the band scales as Φ^v/A^{v-1} when $A \gg \Phi$, the v quanta are localized in the vicinity of the excited site over a timescale which increases with both the local nonlinearity and the number of quanta. This localized behaviour, which is the quantum signature of the classical self-trapping, disappears in the long time limit due to the non vanishing dispersion of the soliton band.

In that context, the aim of the present paper is to analyze the way this scenario is modified when the nonlocal nonlinearity is turned on.

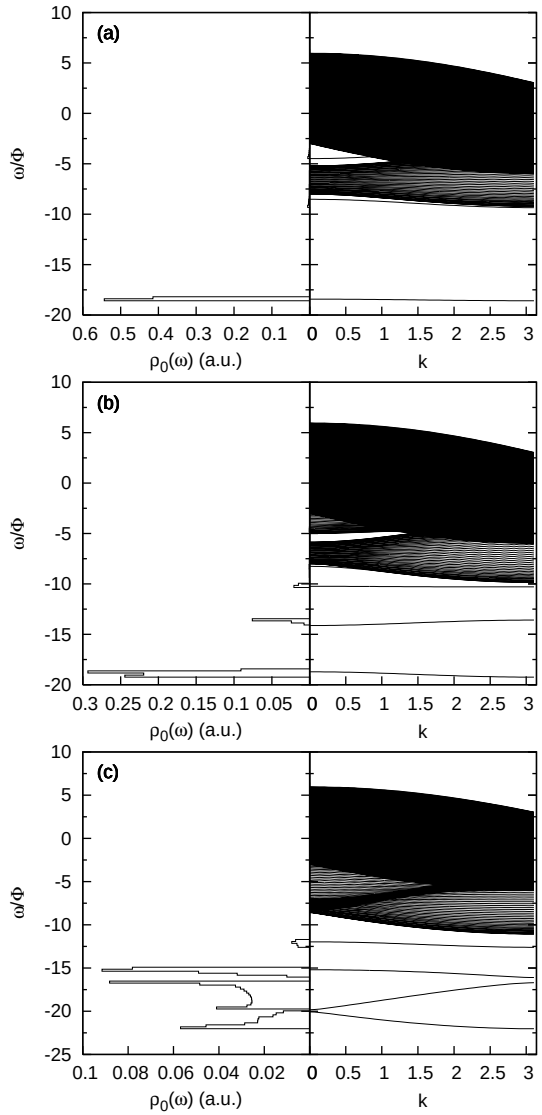

Fig. 1. Energy spectrum for $N = 91$, $v = 3$ and $A = 3\Phi$ and for (a) $B = 0$, (b) $B = 3\Phi$ and (c) $B = 6\Phi$. The left-hand side of the figure represents the corresponding local density of state (see the text).

3 Numerical results

In this section, the numerical diagonalization of the Hamiltonian H is performed and the time dependent Schrödinger equation is solved. To realize the simulation, the hopping constant Φ is used as a reduced unit and the local nonlinearity is fixed to $A = 3\Phi$. The nonlocal nonlinearity is taken as a free positive parameter.

When $v = 3$, the energy spectrum of the Hamiltonian H is displayed in Fig. 1 for $B = 0$ (Fig. 1a), $B = 3\Phi$ (Fig. 1b) and $B = 6\Phi$ (Fig. 1c). In each figure, the spectrum is centred onto the frequency $3\omega_0$ and it corresponds to the dispersion curves drawn in half of the first Brillouin zone of the lattice, i.e. $0 < k < \pi$. The left-hand side of Fig. 1 represents the corresponding local

density of state (LDOS). It describes the weight of the initial state $|\Psi(0)\rangle$ in the eigenstates the energy of which ranges between ω and $\omega + d\omega$ as

$$\rho_0(\omega) = \sum_{k\lambda} |\langle \Psi_\lambda^{(3)}(k)|\Psi(0)\rangle|^2 \delta(\omega - \omega_\lambda^{(3)}(k)) \tag{6}$$

When $B = 0$ (Fig. 1a), the energy spectrum exhibits two energy continua and three isolated bands. The high frequency continuum characterizes free states describing three independent quanta. The low frequency continuum supports states in which two quanta are trapped on the same site whereas the third quantum propagates independently. By contrast, the isolated bands refers to bound states. The low frequency band is the well known soliton band. It lies below the continua over the entire Brillouin zone and it characterizes three quanta trapped on the same site and delocalized along the lattice. The two other bands, which lie respectively below and above the low frequency continuum, describe bound states in which two quanta are trapped on a given site, whereas the third quantum is trapped onto the corresponding nearest neighbour sites. As shown in the left-hand side of Fig. 1a, the LDOS is strongly peaked in the frequency range of the soliton band, which is significantly excited when three quanta are initially created on the same site.

When $B = 3\Phi$ (Fig. 1b), the energy spectrum supports three continua and four isolated bands. Indeed, a third continuum occurs between the two previous energy continua. It describes states for which two quanta are trapped on two nearest neighbour sites whereas the third quantum propagates independently. The low frequency isolated band is the soliton band, whose width has been increased when compared with the previous situation. Above the soliton band, the next two isolated bands correspond to the previously observed bound states in which two quanta are trapped on one site whereas the third quantum is localized on nearest neighbour sites. Note that these bands have been strongly redshifted. Finally, a fourth bound state band occurs just below the continua. The analysis of the corresponding eigenstates reveals that this band supports bound states involving three quanta trapped on three nearest neighbour sites. In addition to the occurrence of this latter band, the behaviour of the LDOS reveals that the non vanishing B value is responsible for a weak hybridization between the three lowest bound state bands. In other words, although the soliton band still mainly refers to three quanta on the same site, the two other bound states involve such a configuration but to a lesser extent.

Finally, when $B = 6\Phi$ (Fig. 1c), the energy spectrum still supports three continua and four isolated bands. The shape of the continua has been slightly modified and the high frequency bound state band, which still mainly refers to three quanta trapped onto three neighbouring sites, has been slightly redshifted. However, strong modifications affect the behaviour of the three low energy bound state bands. Indeed, the gaps between these bands are now very

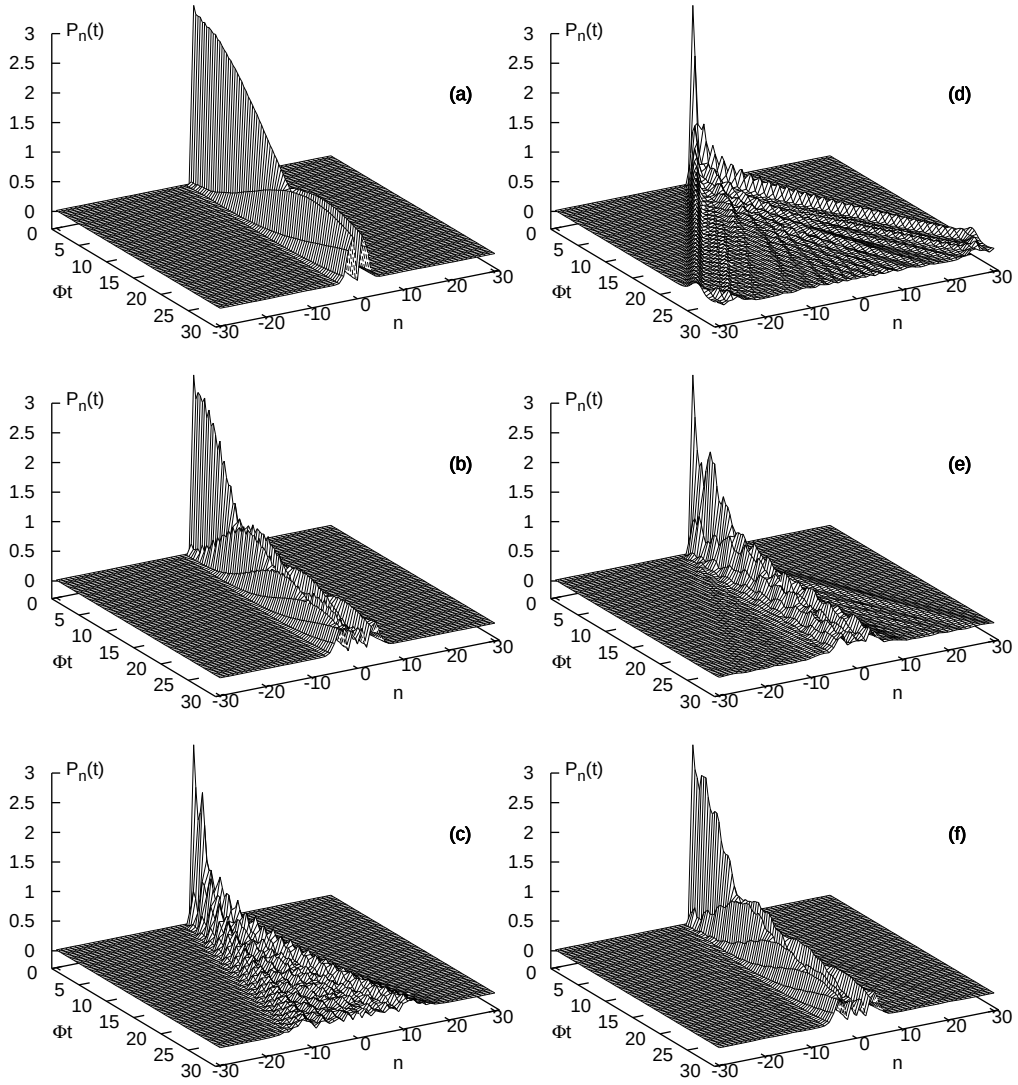

Fig. 2. Space and time evolution of the number of quanta for $N = 91$ and $v = 3$ and for (a) $B = 0$, (b) $B = 2\Phi$, (c) $B = 4\Phi$, (d) $B = 6\Phi$, (e) $B = 8\Phi$ and (f) $B = 10\Phi$

small, which indicates the occurrence of a strong hybridization. The LDOS exhibits a significant value over the frequency range of the three low energy bands. It shows four peaks for specific frequencies, corresponding either to the bottom or to the top of the three low frequency bands (see Fig. 1c). In other words, these bands support bound states which are superpositions of states involving three quanta trapped on one site and two quanta on one site trapped with a third quantum localized on neighbouring sites.

In Fig. 2, the time evolution of the expectation value of the population operator, $P_n(t) = \langle \Psi(t) | b_n b_n^\dagger | \Psi(t) \rangle$, is displayed for $v = 3$ and for different B values. The size of the lattice if fixed to $N = 91$ sites. When $B = 0$ (Fig. 2a), the population of the initial site $P_{n_0}(t)$ decreases very slowly with time. It reaches 50 % of its initial value when t is about $13.5\Phi^{-1}$, which indicates that

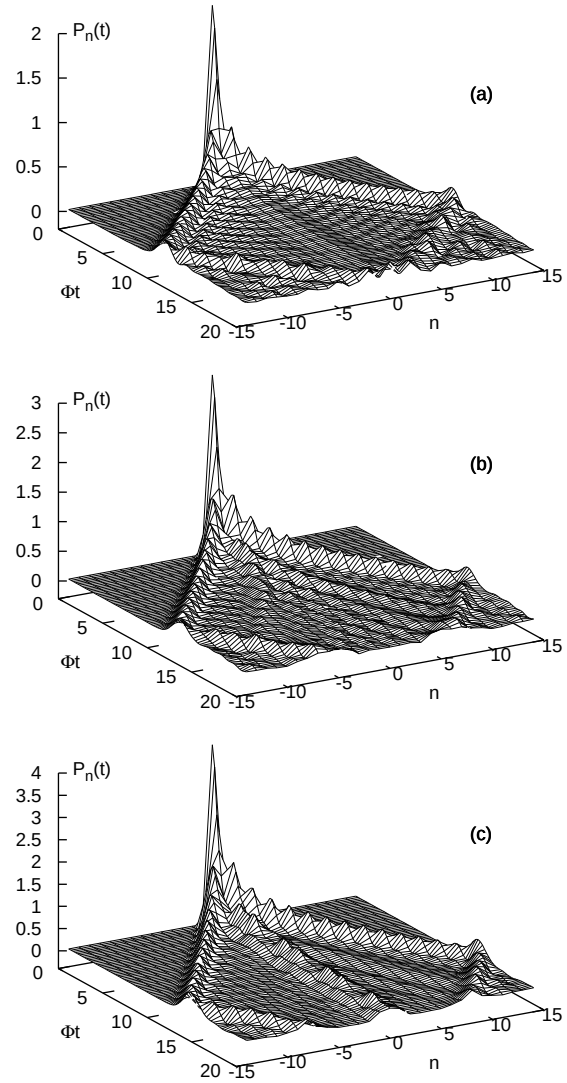

Fig. 3. Space and time evolution of the number of quanta for $N = 29$ and $B = 2A$ and for (a) $v = 2$, (b) $v = 3$ and (c) $v = 4$.

the energy stays localized on the excited site n_0 over a significant timescale. Nevertheless, energy propagation occurs and the population delocalizes along the lattice. However, this propagation corresponds to a rather slow process, since 95 % of the popuplation is concentrated in the 6 sites surrounding n_0 at time $t = 30\Phi^{-1}$. When $B = 2\Phi$ (Fig. 2b), the same features occur. Nevertheless, a faster dynamics takes place since $P_{n_0}(t)$ reaches 50 % of its initial value for $t = 6.8\Phi^{-1}$. The energy propagates slowly and 95 % of the population is concentrated in the 10 sites surrounding n_0 for $t = 30\Phi^{-1}$. When $B = 4\Phi$ (Fig. 2c), the population of the excited site still decays but it now supports high frequency oscillations. Its decay is enhanced, and it reaches 50 % of its initial value when $t = 2.1\Phi^{-1}$. The population propagates more easily along the lattice and its maximum value is observed on the sites $n_0 \pm 12$ for $t = 30\Phi^{-1}$. In that case, 95 % of the population is contained in the 30 sites surrounding n_0.

When $B = 6\Phi$ (Fig. 2d), a fully different behaviour is observed. Indeed, $P_{n_0}(t)$ shows a very fast decay since it reaches 50 % of its initial value for $t = 0.6\Phi^{-1}$. This decay occurs over a timescale of about 20 times shorter than the time associated to the decay of the population for $B = 0$. In addition, Fig. 2d clearly shows that the lattice supports a rather fast energy propagation. Two population wave packets are emitted on each side of the initial site with a velocity of about Φ. In other words, the maximum value of the population is observed on the sites $n_0 \pm 35$ for $t = 30\Phi^{-1}$.

Finally, for greater B values, a rather slow dynamics recurs. When $B = 8\Phi$ (Fig. 2e) and $B = 10\Phi$ (Fig. 2f), the population of the excited site slowly decreases. It supports a small amplitude high-frequency modulation, and it reaches 50 % of its initial value for $t = 4.2\Phi^{-1}$ and $t = 6.3\Phi^{-1}$ when $B = 8\Phi$ and $B = 10\Phi$, respectively. The population propagates along the lattice with a rather small velocity. Therefore, when $t = 30\Phi^{-1}$, 95 % of the energy is concentrated on the 18 sites surrounding the excited site when $B = 8\Phi$. The size of this region decreases to 14 sites when $B = 10\Phi$.

Fig. 2 has clearly shown the occurrence of a specific dynamics when the relation $B = 2A$ is verified. As illustrated in Fig.3, such a behaviour does not depend significantly on the value of the number of quanta. Indeed, the figure shows the time evolution of the population for $v = 2$ (Fig. 3a), $v = 3$ (Fig. 3b) and $v = 4$ (Fig. 3c) and for $B = 2A$. Note that the lattice size is fixed to $N = 29$ to avoid an overlong computational time, especially when $v = 4$. Whatever the number of quanta, the population of the excited site decays over a short timescale. Then, two population wave packets are emitted on each side of the excited site with a velocity which slightly decreases with the number of quanta. When $v = 2$, the wave packets reach the edges of the lattice for $t = 10.8\Phi^{-1}$ whereas longer delays $t = 12.6\Phi^{-1}$ and $t = 13.7\Phi^{-1}$ are required when $v = 3$ and $v = 4$, respectively.

The time evolution of the survival probability is displayed in Fig. 4 for $v = 2$ (Fig. 4a), $v = 3$ (Fig. 4b) and $v = 4$ (Fig. 4c). The number of sites is fixed to $N = 29$ and three different B values have been used, i.e. $B = 0$ (full line), $B = 3\Phi$ (dashed line) and $B = 6\Phi$ (dotted line). The survival probability $S_0(t)$ is defined as the probability to observe the lattice in the state $|\Psi(0)\rangle$ at time t, i.e. $S_0(t) = |\langle\Psi(0)|\Psi(t)\rangle|^2$. It is expressed in terms of the Fourier transform of the LDOS (Eq.(6)) as

$$S_0(t) = |\int_{-\infty}^{+\infty} \rho_0(\omega) e^{-i\omega t} d\omega|^2 \tag{7}$$

When $B = 0$, the survival probability slowly decreases with time, which indicates that the energy is localized on the excited site over a significant timescale

which increases with v. For instance, the first zero of $S_0(t)$ is reached for $t = 4\Phi^{-1}$ and $t = 30\Phi^{-1}$ when $v = 2$ and 3, respectively. When $v = 4$, $S_0(t)$ is almost constant over the timescale displayed in the figure. Note that $S_0(t)$ supports a small amplitude high-frequency modulation which is clearly seen for $v = 3$ and $v = 4$. As when increasing B, $S_0(t)$ exhibits a faster decay. When $B = 3\Phi$, the first zero of the survival probability occurs for $t = 2.4\Phi^{-1}$ and $t = 9.4\Phi^{-1}$ when $v = 2$ and 3, respectively. In a similar way, although the first zero cannot be observed for $v = 4$, $S_0(t)$ decreases with time (Fig. 4c). In a marked contrast with the case $B = 0$, the amplitude of the modulation increases with B. Finally, when $B = 6\Phi$, $S_0(t)$ suddenly shows a very fast decay whatever the number of quanta. This decay occurs over a similar timescale and a first minimum is reached for $t = 0.9\Phi^{-1}$, $t = 0.75\Phi^{-1}$ and $t = 0.7\Phi^{-1}$ when $v = 2$, 3 and 4, respectively. In addition, due to the small lattice size, a revival is observed for $t = 20\Phi^{-1}$, $t = 25\Phi^{-1}$ and $t = 27\Phi^{-1}$ when $v = 2$, 3 and 4, respectively. These latter times represent the delay for the excitation to cover the whole lattice, so that the corresponding velocities are about 1.44Φ, 1.16Φ and 1.06Φ. Therefore, in a perfect agreement with the results observed in Fig. 3, this feature indicates that when $B = 2A$ a fast energy propagation occurs. The initial excitation covers the lattice over a timescale almost independent on the number of quanta and with a velocity typically of the order of the velocity of a single quantum insensitive to any nonlinearity.

To determine the relevant number states which contribute significantly to the quantum dynamics, we introduce $W_\alpha(t)$ as the sum over k of the weight of each intermediate basis vector $|\Phi_\alpha(k)\rangle$ as

$$W_\alpha(t) = \sum_k |\langle \Phi_\alpha(k)|\Psi(t)\rangle|^2 \tag{8}$$

Since a number state refers to a given distribution of the quanta, the associated momentum vector characterizes all the local states connected to that distribution but related to each other through a translation along the lattice. Therefore, the sum over k allows us to characterize the participation of such a distribution in the quantum dynamics. For instance, from the N local vectors $|v, 0, ..., 0\rangle$, ... , $|0, 0, ..., v\rangle$, we have defined in Eq.(2) the vector $|\Phi_1(k)\rangle$ which basically describes v quanta trapped on the same site. The corresponding weight $W_1(t)$ allows us to quantify the participation of such a configuration.

For $v = 3$, Fig. 5 displays the relevant number states involved in the quantum dynamics for $B = 0$ (Fig. 5a), $B = 3\Phi$ (Fig. 5b) and $B = 6\Phi$ (Fig. 5c). When $B = 0$, the states involving 3 quanta trapped on the same site control more than 90 % of the quantum dynamics. However, as when increasing B, the participation of other states takes place. When $B = 3\Phi$ (Fig. 5b), the states describing 3 quanta trapped on the same site remain the most relevant since they carry about 75 % of the full dynamics. However, about 22 % of the

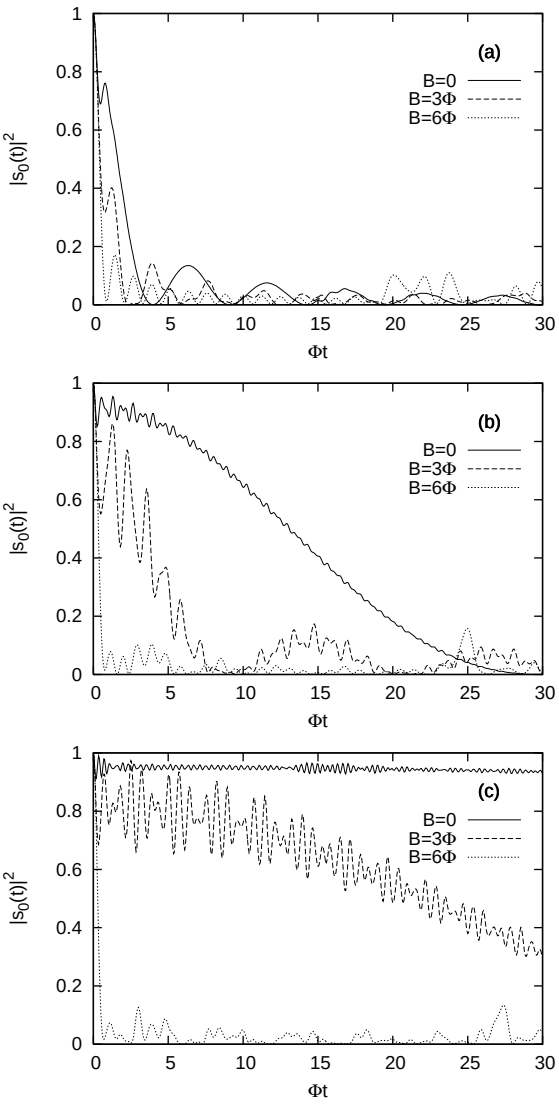

Fig. 4. Survival probability for $N = 29$ and for (a) $v = 2$, (b) $v = 3$ and (c) $v = 4$. Three B values have been used, i.e. $B = 0$ (full line), $B = 3\Phi$ (dashed line) and $B = 6\Phi$ (dotted line).

dynamics is controlled by states involving two quanta on one site trapped to a third quantum located on the nearest neighbour site. A factor 2 is included, due to the participation of the two equivalent states $|2100...\rangle$ and $|1200...\rangle$. Finally, when $B = 6\Phi$ (Fig. 5c), the dynamics are mainly controlled by the states referring to two quanta on one site trapped to a third quantum. These states, including the factor two, carry about 56 % of the full dynamics whereas 35 % originates in states involving 3 quanta trapped on one site. Note that a third type of states connected to three quanta trapped onto three nearest neighbour sites participate to a lesser extent, since they share only 8 % of the dynamics.

Finally, the different observed features are illustrated in Fig. 6 for $v = 5$. The lattice size is fixed to $N = 19$ to avoid an overlong computational time. Nevertheless, Fig. 6a shows the occurrence of the delocalization of the population when $B = 2A$. As when $v = 2$, 3, and 4, a fast decay of the population of

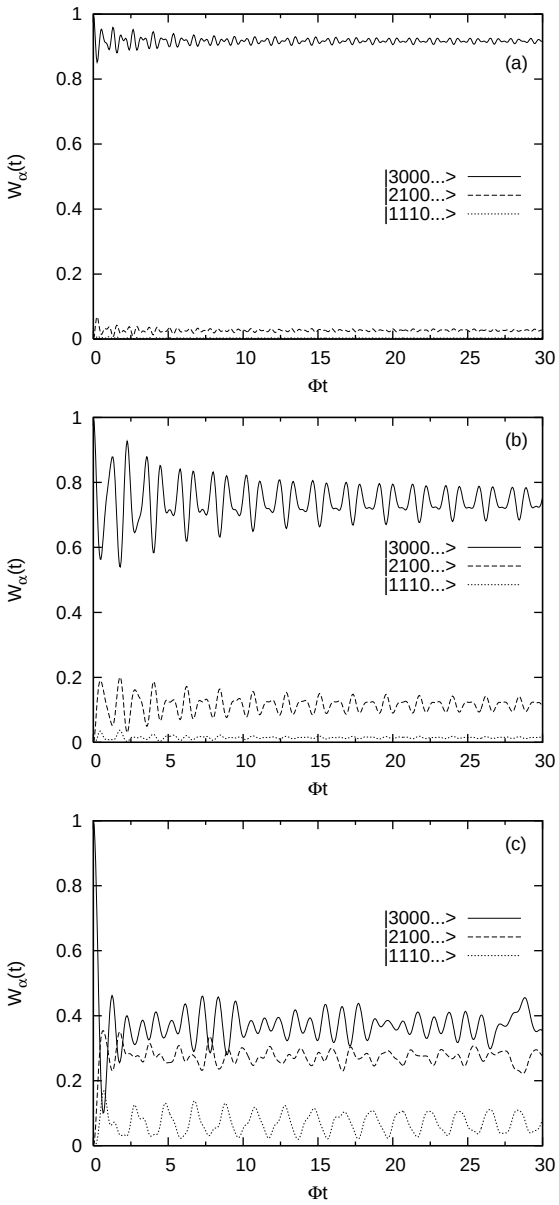

Fig. 5. Relevant number states involved in the quantum dynamics for (a) $B = 0$, (b) $B = 3\Phi$ and (c) $B = 6\Phi$.

the excited site takes place. It is followed by the emission of two wave packets which propagate according to velocity of about Φ. In Fig. 6b, the survival probability indicates a strong energy localization when $B = 0$ and $B = 3\Phi$, whereas it decreases rapidly over a timescale of about $0.5\Phi^{-1}$ when $B = 2A$. Finally, Fig. 6c shows that the main part of the quantum dynamics is described by the states involving the configurations $|500...\rangle$ (about 26 %), $|410...\rangle$ and $|140...\rangle$ (about 40 %), $|320...\rangle$ and $|230...\rangle$ (about 22 %) and $|131...\rangle$ (about 8 %).

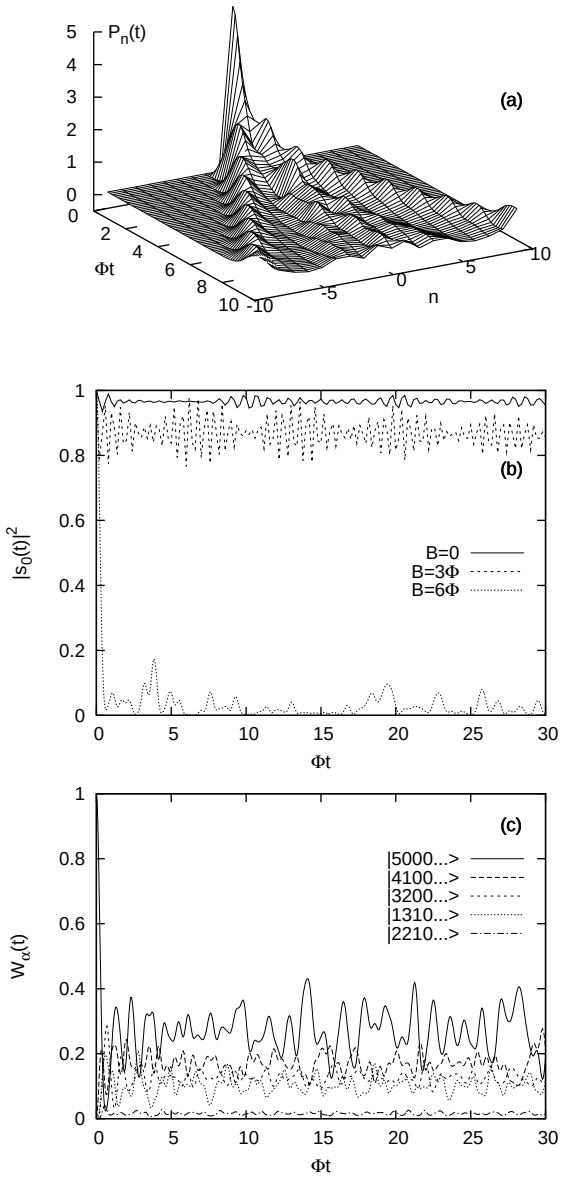

Fig. 6. Lattice dynamics for $v = 5$ and $N = 19$. (a) Space and time evolution of the number of quanta, (b) survival probability and (c) relevant number states.

4 Interpretation and discussion

In the previous section, the numerical results have revealed a strong dependence of the lattice dynamics on the nonlocal nonlinearity B. Indeed, for a vanishing B value, the creation of v quanta on one site mainly excites the soliton band of the energy spectrum. This excitation gives rise to the occurrence of the quantum equivalent of the classical self-trapping phenomena. The energy is localized on the excited site over a significant timescale, which increases with both the local nonlinearity and the number of quanta. Then, a rather slow energy flow takes place due to the finite value of the soliton bandwidth. As when increasing the nonlocal nonlinearity, a faster dynamics occurs. The survival probability, which characterizes the memory of the initial state

in the time dependent quantum state, decreases more rapidly and supports a significant high frequency modulation. Similarly, the population propagates more rapidly along the lattice. In that regime, the speed of the dynamics still depends on the number of quanta and the larger is the number of quanta, the slower is the dynamics. However, when the nonlocal nonlinearity reaches the critical value $B = 2A$, a very different behaviour takes place. Indeed, the lattice supports a very fast energy propagation whose dynamics is almost independent of the number of quanta. The survival probability decreases over a timescale of about Φ^{-1}, and two population wave packets emitted on each side of the excited site propagate with a velocity typically of about Φ. Our numerical results have clearly established that this fast energy transfer is mediated by bound states. However, the timescale of the dynamics is of the same order of magnitude as the timescale governing the free state dynamics. In other words, the bound states involved in the dynamics when $B = 2A$ behave like independent quanta insensitive to the nonlinearity. Finally, when B exceeds its critical value, the quantum self-trapping regime recurs.

As shown in Section 3, the main part of the dynamics is controlled by specific number states. Indeed, we have verified numerically for $v = 2, ..., 7$ that the most relevant states involve number states of the form $|v-p, p, 0, ..., 0\rangle$, with $p = 0, .., v-1$. Note that the states $|1, v-2, 1, ..., 0\rangle$, $|1, v-3, 2, ..., 0\rangle$ and $|2, v-3, 1, ..., 0\rangle$ participate to a lesser extend in the dynamics. Therefore, the relevant states, which describe $v-p$ quanta on one site trapped with p quanta on a nearest neighbour site, are characterized by the self-energies $\epsilon_p = v\omega_0 - v(v-1)A + p(v-p)(2A-B)$ (see Eq.(1)). As long as $|2A-B|$ is strong enough, the different relevant configurations are weakly coupled to each other. Therefore only the number states $|v, 0, 0, ..., 0\rangle$ participate significantly to the dynamics which follows the initial creation of v quanta on one site. However, as illustrated in Fig. 5, a strong hybridization between the different configurations occurs when $|2A-B|$ tends to zero. Finally, when $B = 2A$, a resonance takes place since all the relevant states have the same energy.

To understand more clearly the way this resonance modifies the energy transfer in the nonlinear lattice, we can take advantage of the fact that only relevant number states participate in the full dynamics. This feature allows us to establish a simplified model, which is able to account for the dynamics in the case $A \gg \Phi$. This model is introduced in the next section.

4.1 Equivalent lattice model

As mentioned previously, a good description of the dynamics in the subspace E_v is obtained by restricting the number state basis to the set of the relevant

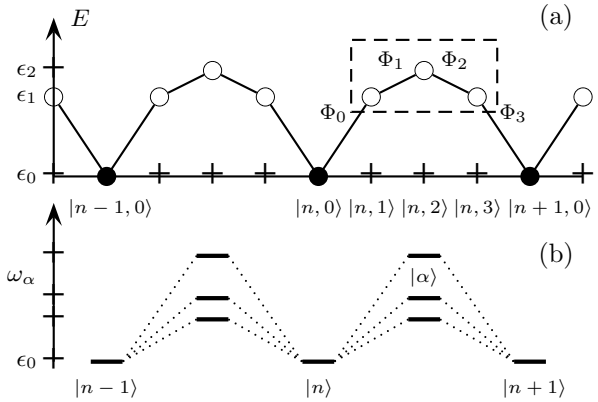

Fig. 7. Equivalent lattice model.

vectors. This set is formed by the $N \times v$ vectors defined as

$$|n,p\rangle = |p_1 = 0, p_2 = 0, ..., p_n = v - p, p_{n+1} = p, ...0\rangle \tag{9}$$

where $|n,p\rangle$ characterizes $v-p$ quanta on the nth site and p quanta of the site $n+1$. The representation of the Hamiltonian H in the restricted basis is equivalent to a tight-binding model on the lattice displayed in Fig. 7a. To simplify the notation, the restriction of the full Hamiltonian will still be denoted H. Within this model, each site supports the state $|n,p\rangle$ whose energy is $\epsilon_p = p(v-p)\epsilon$, where $\epsilon = 2A - B$. Note that $\epsilon_0 = 0$ has been used as the origin of the energy. Nearest neighbour sites are coupled to each other through generalized hopping constants. The hopping constant between $|n,p\rangle$ and $|n,p+1\rangle$ is equal to $\Phi_p = \sqrt{(p+1)(v-p)}\Phi$, with $p = 0, .., v-2$. By symmetry, the hopping constant between $|n, v-1\rangle$ and $|n+1, 0\rangle$ is $\Phi_0 = \sqrt{v}\Phi$.

Consequently, the dynamics of the quantum nonlinear lattice is formally equivalent to the dynamics of a fictitious particle moving on the lattice shown in Fig. 7a. At time $t = 0$, the particle is created in the state $|n_0, 0\rangle$ and its time evolution is governed by the corresponding Schrödinger equation. Unfortunately, although the model has been greatly simplified, this equation cannot be solved analytically. However, the knowledge of some general properties is sufficient to clarify our understanding of the physics involved in the energy transfer. In addition, the model allows us to determine the LDOS which characterizes the weight of a localized state $|n, 0\rangle$ in the eigenstates of the lattice. It represents a measure of the response of the lattice to the initial excitation and gives the survival probability simply by performing a Fourier transform.

4.2 General properties of the lattice eigenstates

The lattice displayed in Fig. 7a exhibits a translational invariance and its unit cell is defined in terms of two subsystems. The first subsystem is formed

by the single state $|n,0\rangle$, whereas the second subsystem involves the $v-1$ coupled states $|n,p\rangle$, with $p=1,..,v-1$. A moment's reflection will convince the reader that this latter subsystem represents a modified nonlinear quantum dimer. More precisely, it is the representation of a dimer in the number state basis in which the two states involving v quanta on the first site and v quanta on the second site have been suppressed. As for the dimer, this subsystem is invariant under the reflection symmetry which transforms the state $|n,p\rangle$ into the state $|n,v-p\rangle$.

Due to the translational invariance, the lattice wave vector k is a good quantum number. Therefore, for each k value, the quantum states are described by a $v\times v$ matrix $H(k)$. Instead of representing this matrix in the local basis $|n,p\rangle$, it is more convenient to introduce a new basis set formed by the single state $|n,0\rangle$ and by the $v-1$ eigenstates of the modified dimer. Indeed, although the quantum states of a modified dimer are only known for small v values, they represent a key ingredient needed to understand the physics of the lattice. Therefore, let $|\alpha\rangle$ denotes the αth eigenstate of a modified dimer whose energy is ω_α (see Fig. 7b). Because of the reflection symmetry, each eigenstate is either symmetric or antisymmetric. As a result, the wave function $\psi_{\alpha p}=\langle n,p|\alpha\rangle$ satisfies $\psi_{\alpha p}=\pm\psi_{\alpha v-p}$, depending on whether the state is symmetric $(+)$ or antisymmetric $(-)$. For even v values, there are $N_S=v/2$ symmetric and $N_A=(v-2)/2$ antisymmetric eigenstates. By contrast, for odd v values, $N_S=N_A=(v-1)/2$.

In that context, the matrix Hamiltonian $H(k)$ is expressed as

$$H(k)=\begin{pmatrix} 0 & x_\alpha(k) & x_{\alpha'}(k) & ... \\ x_\alpha^*(k) & \omega_\alpha & 0 & ... \\ x_{\alpha'}^*(k) & 0 & \omega_{\alpha'} & ... \\ ... & ... & .... & ... \end{pmatrix} \tag{10}$$

where $x_\alpha(k)=\sqrt{v}\phi(\psi_{\alpha 1}+\psi_{\alpha v-1}\exp(-ik))$ is the coupling between the state $|n,0\rangle$ and $|\alpha\rangle$ which results from the interaction between $|n,0\rangle$ with both the state $|n,1\rangle$ of the same unit cell and the state $|n-1,v-1\rangle$ of the previous unit cell (see Fig. 7).

¿From Eq.(10), the delocalization of the fictitious particle originates in the coupling between two neighbouring states $|n,0\rangle$ and $|n+1,0\rangle$, through their interaction with the eigenstates of the nth modified dimer. As a consequence, each lattice eigenstate is a superimposition involving the localized states and the eigenstates of a modified dimer. However, such a hybridization depends both on the energy difference ω_α, and on the strength of the coupling $x_\alpha(k)$, which is drastically sensitive to the symmetry of the dimer eigenstates.

Eq.(10) allows us to determine the exact expression of the LDOS. Indeed, according to the standard definition used in condensed matter physics, the LDOS is expressed in terms of the Green's operator $G(k,\omega) = (\omega - H(k))^{-1}$ as

$$\rho_0(\omega) = -\frac{1}{N\pi} Im \sum_k \langle n_0, 0|G(k, \omega + i0^+)|n_0, 0\rangle \tag{11}$$

Since the LDOS only depends on the restriction of the Green's operator to $|n_0, 0\rangle$, it can be obtained by applying standard projection methods. Therefore, by taking advantage of the symmetry of the eigenstates $|\alpha\rangle$, the restricted Green's operator is written as

$$\langle n_0, 0|G(k,\omega)|n_0, 0\rangle = \frac{1}{\omega - \Delta(\omega) - 2J(\omega)\cos(k)} \tag{12}$$

where

$$\begin{aligned} \Delta(\omega) &= 2v\Phi^2 \sum_\alpha \frac{\psi_{\alpha 1}\psi_{\alpha 1}}{\omega - \omega_\alpha} \\ J(\omega) &= v\Phi^2 \sum_\alpha \frac{\psi_{\alpha 1}\psi_{\alpha v-1}}{\omega - \omega_\alpha} \end{aligned} \tag{13}$$

By inserting Eq.(12) into Eq.(11), the LDOS is finally written as

$$\rho_0(\omega) = \frac{1}{\pi} \frac{1}{\sqrt{(2J(\omega) + \Delta(\omega) - \omega)(2J(\omega) - \Delta(\omega) + \omega))}} \tag{14}$$

Eq.(14) allows us to establish two general properties. First, the zeros of the LDOS are given by the poles of the parameters $\Delta(\omega)$ and $J(\omega)$. In that context, Eq.(13) clearly shows that the LDOS supports $v-1$ zeros, which corresponds to the eigenenergies of the modified dimer. In the vicinity of a zero, the LDOS scales as $\sqrt{|\omega - \omega_\alpha|}$. Then, the LDOS exhibits two kinds of poles which are given by the solutions of the two equations $2J(\omega) \pm (\Delta(\omega) - \omega) = 0$. From Eq.(13), these two equations are rewritten as

$$\begin{aligned} 4v\Phi^2 \sum_\alpha^S \frac{\psi_{\alpha 1}^2}{\omega - \omega_\alpha} &= \omega \\ 4v\Phi^2 \sum_\alpha^A \frac{\psi_{\alpha 1}^2}{\omega - \omega_\alpha} &= \omega \end{aligned} \tag{15}$$

where the symbol $\sum^{S,A}$ denotes a sum over either the symmetric or the anti-symmetric eigenstates of a modified dimer. In Eq.(15), the first equation gives

$N_S + 1$ solutions whereas the second equation yields $N_A + 1$ solutions. Therefore, the LDOS supports $N_S + N_A + 2 = v + 1$ poles. In the vicinity of a pole ω_{po}, the LDOS thus diverges according to the power law $|\omega - \omega_{po}|^{-1/2}$.

These results reveal the occurrence of zeros and poles in the LDOS, as observed in Fig. 1. In addition, they point out the important role of the symmetry of the eigenstates of the dimer, especially for specific values of the lattice wave vector k. Indeed, when $k = 0$, the coupling $x_\alpha(k = 0)$ between $|n, 0\rangle$ and each antisymmetric state $|\alpha\rangle$ vanishes. As a consequence, $H(k = 0)$ (Eq.(10)) has N_A eigenvalues equal to the eigenenergies of the antisymmetric states of the modified dimer. They describe lattice eigenstates which do not involve $|n, 0\rangle$, so they corresponds to zeros of the LDOS. By contrast, the remaining coupling between $|n, 0\rangle$ and the symmetric states $|\alpha\rangle$ produces N_S+1 eigenstates which induce divergences in the LDOS. When $k = \pi$, the same features occur, but by inverting the role played by the symmetric and the antisymmetric states. The matrix $H(k = \pi)$ exhibits N_S eigenvalues equal to the eigenenergies of the symmetric states $|\alpha\rangle$ and which correspond to zeros of the LDOS. A strong coupling remains between $|n, 0\rangle$ and the N_A antisymmetric states, leading to $N_A + 1$ eigenvalues which give rise to divergences in the LDOS.

Finally, the coupling between $|n, 0\rangle$ and the $v - 1$ dimer eigenstates $|\alpha\rangle$ is at the origin of the creation of the lattice eigenstates. It is responsible for the occurrence of specific signatures in the LDOS and control the lattice dynamics. However, depending on the strength of the coupling, different dynamical behaviours can be observed ranging from quantum self-trapping to fast energy transfer. In the following of the text, these features are first illustrated for the two simples situations corresponding to $v = 2$ and $v = 3$. Then, a general discussion is given to interpret the specific behaviour observed when $\epsilon = 0$.

4.3 Application to $v = 2$ and $v = 3$

The case $v = 2$ is rather simple, because a modified dimer involves a single state $|n, 1\rangle$ whose energy is $\epsilon_1 = \epsilon$. Therefore, $H(k)$ is a 2×2 matrix which describes the hybridization between $|n, 0\rangle$ and $|n, 1\rangle$. It can be solved exactly so that the lattice supports two bands whose dispersion relations are expressed as

$$E_\pm(k) = \frac{\epsilon}{2} \pm \sqrt{(\frac{\epsilon}{2})^2 + 8\Phi^2 \cos^2(k/2)} \tag{16}$$

The corresponding LDOS, which shows a single zero and three poles, is defined as

$$\rho_0(\omega) = \frac{1}{\pi}\sqrt{\frac{-(\omega-\epsilon_1)}{(\omega-E_-(0))(\omega-E_-(\pi))(\omega-E_+(0))}} \tag{17}$$

When $\epsilon \gg \Phi$ ($B \ll 2A$), the two bands are only weakly coupled. The low frequency band, whose energy is about $\epsilon_0 = 0$, refers to the delocalization of the fictitious particle over the different states $|n,0\rangle$. By contrast, the second band accounts for the delocalization of the fictitious particle over the states $|n,1\rangle$. In other words, the low frequency band is the soliton band describing two quanta trapped on the same site and delocalized along the lattice. The second band refers to the delocalization of bound states involving two quanta trapped onto two nearest neighbour sites.

Since only the soliton band is significantly excited, it controls the dynamics. To understand this feature, let us evaluate the corresponding survival probability (Eq.(7)). Although the Fourier transform of Eq.(17) is not analytic in a general way, it can be evaluated when the two bands lie far from each other. In that case, the integral over the frequency range of a given band can be performed by neglecting the frequency dependence of the other band. After straightforward calculations, the survival probability is thus expressed as

$$S_0(t) \approx J_0^2(\frac{4\Phi^2 t}{\epsilon})[1-\frac{8\Phi^2}{\epsilon^2}(1-\cos(\epsilon t))] \tag{18}$$

where J_0 is the Bessel function of the first kind. The survival probability slowly decreases with time and it reaches its first zero for $t = 2.4\epsilon/4\Phi^2$. Note that this value is extracted from the first zero $t \approx 2.40$ of $J_0(t)$. When $A = 3\Phi$ and $B = 0$, this value is equal to $3.6\Phi^{-1}$, in a perfect agreement with the numerical results about $4\Phi^{-1}$ (see Fig. 4a). Eq.(18) shows that the survival probability supports a high frequency modulation whose amplitude decreases with ϵ. Such a modulation, whose frequency is equal to the energy difference between $|n,0\rangle$ and $|n,1\rangle$, characterizes the small participation of the second band in the dynamics.

As when ϵ decreases, i.e. when B tends to $2A$, the width of the low frequency band increases as a result of the redshift of its low frequency edge. By contrast, the second band exhibits a strong redshift accompanied by an increase in width. In addition, its contribution to the LDOS increases, which indicates that the coupling between the two kinds of bound states is enhanced. Such a behaviour occurs until the high frequency edge of the soliton band meets the low frequency edge of the second band. This feature takes place when $\epsilon = 0$, i.e. when $B = 2A$. In that case, the LDOS displays a single band, only, with

two divergences whose frequencies are $\pm 2\sqrt{2}\Phi$. The corresponding bandwidth is thus a maximum and it is equal to $4\sqrt{2}\Phi$. At the resonance, this band clearly suggest strong hybridization between $|n,0\rangle$ and $|n,1\rangle$. In that case, the Fourier transform of Eq.(17) can be determined exactly and it yields the following survival probability

$$S_0(t) = J_0^2(2\sqrt{2}\Phi t) \tag{19}$$

The resonance induces a decay of the survival probability over a very short timescale. It reaches its first zero for $t = 0.85\Phi^{-1}$, in perfect agreement with the results shown in Fig. 4a. This feature, mainly due to the strong hybridization between the two bands, is responsible for a fast energy transfer along the whole lattice. In other words, the transport of energy results from a series of transitions between states involving successively two quanta on the same site and two quanta on nearest neighbour sites.

When $v = 3$, a modified dimer involves the two states $|n,1\rangle$ and $|n,2\rangle$, which have the same energy 2ϵ. The first state describes two quanta on site n and one quantum on site $n+1$, whereas the second state refers to one quantum on site n and two quanta on site $n+1$. Due to the coupling $\Phi_1 = 2\Phi$ between these states, a strong hybridization takes place so that the eigenstates of the modified dimer correspond to a symmetric and to an antisymmetric superimposition as

$$|\alpha_\pm\rangle = \frac{1}{\sqrt{2}}(|n,1\rangle \pm |n,2\rangle) \tag{20}$$

The corresponding eigenenergies are $\omega_\pm = 2\epsilon \pm 2\Phi$. Therefore, $H(k)$ is a 3×3 matrix which describes the hybridization between $|n,0\rangle$ and $|\alpha_\pm\rangle$. In a general way, the lattice supports three bands and the corresponding LDOS is written as

$$\rho_0(\omega) = \frac{1}{\pi}\sqrt{\frac{-(\omega-\omega_+)(\omega-\omega_-)}{(\omega-E_1)(\omega-E_2)(\omega-E_3)(\omega-E_4)}} \tag{21}$$

where the four poles are defined as

$$\begin{aligned}
E_1 &= \epsilon - \Phi - \sqrt{\epsilon^2 - 2\epsilon\Phi + 7\Phi^2} \\
E_2 &= \epsilon + \Phi - \sqrt{\epsilon^2 + 2\epsilon\Phi + 7\Phi^2} \\
E_3 &= \epsilon - \Phi + \sqrt{\epsilon^2 - 2\epsilon\Phi + 7\Phi^2} \\
E_4 &= \epsilon + \Phi + \sqrt{\epsilon^2 + 2\epsilon\Phi + 7\Phi^2}
\end{aligned} \tag{22}$$

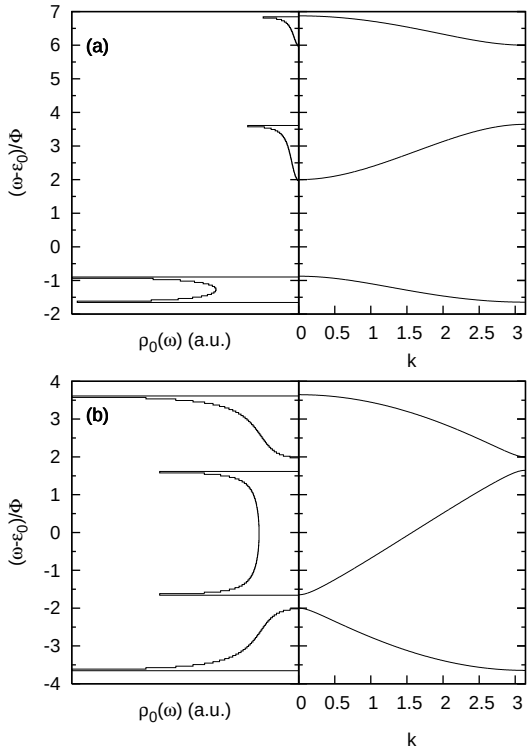

Fig. 8. Theoretical energy spectrum and LDOS for $v = 3$ and for (a) $\epsilon = 2$ and (b) $\epsilon = 0$.

For strong ϵ values (see Fig. 8a), the three bands are well separated, in a perfect agreement with the results displayed in Fig. 1a and 1b. As for $v = 2$, the low frequency band mainly describes the delocalization of the fictitious particle over the different states $|n, 0\rangle$. It thus corresponds to the soliton band, the LDOS of which exhibits two divergences whose frequencies are E_1 and E_2. The resulting bandwidth is thus about $6\Phi^3/\epsilon^2$. By contrast, the two other bands account for the delocalization of the fictitious particle over the eigenstates $|\alpha_\pm\rangle$ belonging to different unit cells. Consequently, the band just above the soliton band refers to bound states formed by the antisymmetric superimposition of the states $|n, 1\rangle$ and $|n, 2\rangle$, whereas the high frequency band characterizes bound states involving their symmetric superimposition. As shown in Fig. 8a, the LDOS connected to these two bands shows a single divergence and a single zero.

Since only the soliton band is significantly excited when three quanta are created on one site, it controls the main part of the dynamics. The survival probability is thus approximately expressed as

$$S_0(t) \approx (1 - \frac{3\Phi^2}{\epsilon^2}) J_0^2(\frac{3\Phi^3 t}{\epsilon^2}) + \frac{3\Phi^2}{\epsilon^2} J_0(\frac{3\Phi^3 t}{\epsilon^2}) [J_0(\frac{3\Phi^2 t}{2\epsilon}) \cos(2\epsilon t) - J_1(\frac{3\Phi^2 t}{2\epsilon}) \sin(2\epsilon t)] \cos(2\Phi t) \qquad (23)$$

The survival probability exhibits a rather slow dynamics governed by the first term in the right-hand side of Eq.(23). It decreases over a timescale typically of about $t = 2.40\epsilon^2/3\Phi^3$. When $A = 3\Phi$ and $B = 0$, this time is equal to $28.8\Phi^{-1}$, in a perfect agreement with the numerical results $30\Phi^{-1}$ (see Fig. 4b). Note that the survival probability supports a high frequency modulation whose amplitude decreases with ϵ. Such a modulation, whose frequency is typically about $\omega_\pm$, accounts for the small hybridization between the soliton band and the two other bands.

As for the case when ϵ decreases, i.e. when B tends to $2A$, the three bands are redshifted and their bandwidth increases. In addition, the contribution to the LDOS of the two high frequency bands is enhanced due to their hybridization with the soliton band. Nevertheless, the three bands do not hybridize in a similar way. Indeed, the soliton band hybridizes first with the antisymmetric band. This mechanism dominates when $\epsilon = \Phi/4$, for which both the soliton band and the antisymmetric band condense into a single band. Then, for smaller ϵ values, the hybridization with the symmetric band takes place. Finally, when $\epsilon = 0$, the LDOS exhibits three bands again (Fig. 8b). However, all these bands mix the three different kinds of bound states so that the three bands control the dynamics. As a result, the typical time governing the decay of the survival probability is about $t = 2 \times 2.4/\Delta\omega$, where $\Delta\omega = 2(1+\sqrt{7})\Phi$ is the difference between the high frequency and the low frequency divergences of the LDOS. When $A = 3\Phi$ and $B = 6\Phi$, this time is equal to $0.66\Phi^{-1}$ in perfect agreement with the numerical results $0.75\Phi^{-1}$ (see Fig. 4b). As a consequence, a fast energy transfer takes place, with a velocity of about the hopping constant Φ, which characterizes the motion of single quantum insensitive to the nonlinearity. However, as for $v = 2$, the transport of energy is mediated by states formed by the superimposition of the three kinds of bound states.

4.4 Interpretation of the resonance $\epsilon = 0$

The previous examples clearly illustrate the fact that the lattice dynamics exhibits two distinct behaviours, depending on the value of the parameter $\epsilon = 2A - B$.

When $\epsilon \gg \Phi$ ($B \ll 2A$), the energy transfer is mediated by bound states formed by v quanta trapped on the same site and behaving as a single particle. This particle delocalizes along the lattice due to the coupling between nearest neighbour states $|n, 0\rangle$ through their interaction with the modified dimers. Because the eigenenergies of the dimer lie far from the energy of the localized state $|n, 0\rangle$, this coupling is very weak. Consequently, the v quanta bound states belong to the low energy soliton band, which is characterized by a

very small bandwidth of about $\Delta\omega \approx 4v\Phi^v/(v-1)!\epsilon^{v-1}$ [16,17]. Therefore, the creation of v quanta on one site mainly excites the soliton band, leading to the occurrence of the quantum equivalent of the classical self-trapping. The energy is localized on the excited site over a significant timescale which increases with both ϵ and v. It finally propagates slowly at a very small velocity, proportional to the bandwidth.

By contrast, when $\epsilon = 0$, i.e. when $B = 2A$, a very different behaviour takes place, mainly due to the occurrence of a resonance, since all the states $|n, p\rangle$ have the same self-energy. This resonance allows for a complete energy delocalization at a rather large velocity, typically of about the hopping constant Φ. In a marked contrast with the previous situation, the resonance induces a strong interaction between the localized states and the modified dimers. Nevertheless, as detailed below, the origin of this interaction strongly depends on whether v is even or odd, due to the v dependence of the energy spectrum of a modified dimer.

For even v values, a modified dimer supports a single eigenstate, denoted as $|\alpha_0\rangle$, whose energy vanishes. The $v-2$ remaining eigenstates are grouped into pairs formed by two eigenstates having the same symmetry but with opposite energy. As a result, the coupling between $|n, 0\rangle$ and all these $v-2$ eigenstates appears extremely weak. Indeed, by using a standard perturbation theory, it is easy to show that the second order correction of the energy of $|n, 0\rangle$ due to these couplings is expressed as $\Delta E = -\sum_{\alpha\neq\alpha_0} |x_\alpha(k)|^2/\omega_\alpha$. This correction vanishes exactly because the sum involves pairs of states which experience the same interaction with $|n, 0\rangle$ but which have an opposite energy. In other words, a pair of eigenstates yields two pathways for the transition between $|n, 0\rangle$ and $|n+1, 0\rangle$ which interfere destructively so that the resulting probability amplitude vanishes.

Consequently, the relevant part of $H(k)$ reduces to a 2×2 matrix which describes the hybridization between $|n, 0\rangle$ and the resonant eigenstate $|\alpha_0\rangle$. From Eq.(10), it can be solved exactly so that the lattice supports two energy bands whose dispersion relations are expressed as $\pm\sqrt{v}\Phi|\psi_{\alpha_0 1} + \psi_{\alpha_0 v-1}\exp(-ik)|$. Depending on whether $|\alpha_0\rangle$ is symmetric or antisymmetric, these two bands vanish for $k = \pi$ or $k = 0$. Therefore, the gap between these two bands vanishes, so that the resulting bandwidth is equal to $\Delta\omega = 4\sqrt{v}\Phi|\psi_{\alpha_0 1}|$. By performing the numerical diagonalization of the dimer Hamiltonian for v ranging from 2 to 200, it is straightforward to show that the wave function behaves as $|\psi_{\alpha_0 1}| \approx \sqrt{2/v}$. The bandwidth is thus of about a few times the hopping constant as $\Delta\omega \approx 4\sqrt{2}\Phi$. Note that the diagonalization of the full $H(k)$ matrix Eq.(10) shows that the bandwidth slightly decreases with the number of quanta. For instance it varies from 5.66Φ for $v = 2$ to 4.50Φ for $v = 50$. This rather large bandwidth is responsible for the decay of the survival probability over a short timescale, which indicates the occurrence of a fast energy transfer

at a velocity typically of about the velocity of independent quanta insensitive to the nonlinearity. Nevertheless, this delocalization originates in the propagation of bound states, which result from the hybridization between v-quanta trapped on the same site and v-quanta distributed according to the resonant state $|\alpha_0\rangle$. Our numerical analysis reveals that this distribution involves the superimposition of the number states $|v-1,1,0,0...\rangle$, $|v-3,3,0,0...\rangle$, $|v-5,5,0,0...\rangle$ ...$|1,v-1,0,0...\rangle$.

For odd v values, the modified dimer has $v-1$ eigenstates which are grouped into pairs containing two states having an opposite energy and a different symmetry. Therefore, since no resonance occurs with the modified dimer, $|n,0\rangle$ interacts with all the eigenstates $|\alpha\rangle$. Nevertheless, among all these interactions, only the coupling between $|n,0\rangle$ and the two eigenstates whose energy is close to zero is significant. These two states, denoted by $|\alpha_S\rangle$ (symmetric) and $|\alpha_A\rangle$ (antisymmetric) respectively, belong to the same group and have an opposite energy $\omega_S = -\omega_A$. Consequently, the relevant part of the $H(k)$ reduces to a 3×3 matrix written as

$$H(k) \approx \begin{pmatrix} 0 & x_S(k) & x_A(k) \\ x_S^*(k) & \omega_S & 0 \\ x_A^*(k) & 0 & -\omega_S \end{pmatrix} \tag{24}$$

where $x_S(k) = \sqrt{v}\Phi\psi_{S1}(1+\exp(-ik))$ and $x_A(k) = \sqrt{v}\Phi\psi_{S1}(1-\exp(-ik))$. As discussed in Section 4.2, Eq.(24) can be diagonalized for specific values of the lattice wave vector k by taking advantage of the dimer eigenstate symmetry. Indeed, when $k=0$, the coupling between $|n,0\rangle$ and $|\alpha_A\rangle$ vanishes. The energy ω_A is thus an eigenvalue of the matrix Hamiltonian Eq.(24) which corresponds to a zero of the LDOS. However, the coupling between $|n,0\rangle$ and $|\alpha_S\rangle$ remains and it produces two eigenvalues $\omega_S/2 \pm \sqrt{(\omega_S/2)^2 + 4v\Phi^2|\psi_{S1}|^2}$ which correspond to two poles of the LDOS. In the same way, when $k=\pi$, there is no interaction between $|n,0\rangle$ and the symmetric state so that ω_S is an eigenvalue of the Hamiltonian which is a zero of the LDOS. By contrast, the coupling with the antisymmetric state leads to two eigenvalues $-\omega_S/2 \pm \sqrt{(\omega_S/2)^2 + 4v\Phi^2|\psi_{S1}|^2}$ which yield two poles of the LDOS.

Consequently, the energy spectrum supports three bands which describe strong hybridizations between the three states $|n,0\rangle$, $|\alpha_S\rangle$ and $|\alpha_A\rangle$. These bands govern the dynamics of the lattice which is controlled by a rather large bandwidth defined as the energy difference between the high frequency and the low frequency divergences of the LDOS as $\Delta\omega = |\omega_S| + \sqrt{\omega_S^2 + 16v\Phi^2|\psi_{S1}|^2}$. The numerical analysis reveals that this bandwidth is of about a few times the hopping constant Φ. However, as for even v value, the exact diagonalization of the full $H(k)$ matrix Eq.(10) reveals that the bandwidth slightly decreases

with the number of quanta. It varies from 7.29Φ for $v = 3$ to 6.72Φ for $v = 51$. Therefore, this large bandwidth favours a fast decay of the survival probability followed by a fast energy transfer. This energy transfer is mediated by bound states formed by the superimposition of v-quanta trapped on the same site and v-quanta distributed according to the two states $|\alpha_S\rangle$ and $|\alpha_A\rangle$ which involve all the number states $|v-1,1,0,0...\rangle$, $|v-2,2,0,0...\rangle$, $...|1,v-1,0,0...\rangle$.

Acknowledgements

The authors would like to acknowledge the " Région de Franche-Comté " which has partially supported this work through a BDI Grant.

References

[1] A. S. Davydov, N. I. Kisluka, Phys. Status Solidi 59 (1973) 465; Zh. Eksp. Teor. Fiz 71 (1976) 1090 [Sov. Phys. JETP 44 (1976) 571].

[2] A.C. Scott, Phys. Rep. 217 (1992)1 .

[3] P. L. Christiansen, A. C. Scott , *Davydov's Soliton Revisited*,(Plenum, New York, 1990).

[4] J.C. Eilbeck, P.S. Lomdahl and A.C. Scott, Phys. Rev. B (1984) 4703.

[5] J.C. Eilbeck, P.S. Lomdahl and A.C. Scott, Physica D16 (1985) 318.

[6] A. J. Sievers, S. Takeno, Phys. Rev. Lett. 61 (1988) 970.

[7] S. Aubry, Physica D103 (1997) 201.

[8] S. Flach, C.R. Willis, Phys. Rep. 295 (1998) 181.

[9] R.S. MacKay, Physica A 288 (2000) 174.

[10] V. Fleurov, Chaos 13 (2003) 676.

[11] J. C. Kimball, C. Y. Fong, Y. R. Shen, Phys. Rev. B 23 (1981) 4946.

[12] F. Bogani, G. Cardini, V. Schettino, P. L. Tasselli , Phys. Rev. B 42 (1990) 2307 .

[13] V.Z. Enol'skii, M. Salerno, A.C. Scott, J.C Eilbeck, Physica D 59 (1992) 1.

[14] J.C. Eilbeck, Some exact results for quantum lattice problems in: L. Vasquez, R.S. Mackay, M. P. Zorzano (Eds), Proceedings of the Third Conference Localization and Energy Transfer, in Nonlinear Systems, World Scientific, Singapore, 2003.

[15] E. Wright, J.C Eilbeck, M.H. Hays, P.D. Miller, A.C. Scott, Physica D 69 (1993) 18.

[16] L. Bernstein, J.C. Eilbeck and A.C. Scott, Nonlinearity 3 (1990) 293.

[17] A. C. Scott, J. C. Eilbeck, H. Gilhoj, Physica D 78 (1994) 194.

[18] J. Doriganc, J. C. Eilbeck, M. Salerno, A. C. Scott, Phys. Rev. Lett. 93 (2004) 025504.

[19] L. Proville, Phys. Rev. B 71 (2005) 1043306.

[20] V. Pouthier, J. Chem. Phys. 118 (2003) 3736.

[21] V. Pouthier, J. Chem. Phys. 118 (2003) 9364 .

[22] V. Pouthier, Phys. Rev. E 68 (2003) 021909.

[23] V. Pouthier, C. Falvo, Phys. Rev. E 69 (2004) 041906.

[24] C. Falvo, V. Pouthier, J. Chem. Phys. 123 (2005) 184709.

[25] C. Falvo, V. Pouthier, J. Chem. Phys. 123 (2005) 184710.

[26] V. Pouthier, Phys. Rev. B71 (2005) 115401.

[27] V. Pouthier, Physica D 213 (2006) 1.

[28] P. Guyot-Sionnest, Phys. Rev. Lett. 67 (1991) 2323.

[29] R. Honke, P. Jakob, Y. J. Chabal, A. Dvorak, S.Tausendpfund, W. Stigler, P. Pavone, A. P. Mayer, and U. Schröder, Phys. Rev. B59 (1999) 10996.

[30] R. P. Chin, X. Blase, Y. R. Shen, and S. GT. Louie, Europhys. Lett. 30 (1995) 399.

[31] D. J. Dai and G. E. Ewing, Surf. Sci. 312 (1994) 239.

[32] P. Jakob, Phys. Rev. Lett. 77 (1996) 4229.

[33] P. Jakob, Physica D119 (1998) 109.

[34] P. Jakob, J. Chem. Phys. 114 (2001) 3692.

[35] P. Jakob, Appl. Phys. A75 (2002) 45.

[36] P. Jakob and B.N.J. Persson, J. Chem. Phys. 109 (1998) 8641.

[37] H. Okuyama, T. Ueda, T. Aruga, and M. Nishijima, Phys. Rev. B63 (2001) 233404.

[38] J. Edler, R. Pfister, V. Pouthier, C. Falvo, P. Hamm, Phys. Rev. Lett. 93 (2004) 106405.

[39] G. Kalosakas and A.R. Bishop, Phys. Rev. A 65 (2002) 043616.

[40] G. Kalosakas, A.R. Bishop, and V.M. Kenkre, Phys. Rev. A 68 (2003) 023602.

[41] G. Kalosakas, A.R. Bishop, and V.M. Kenkre, J. Phys. B:At. Mol. Opt. Phys. 36 (2003) 3233.

[42] V. Pouthier, Physica D (submitted).